energies

MDPI

Article

Hybrid Fault-Tolerant Control for Air-Fuel Ratio Control System of Internal Combustion Engine Using Fuzzy Logic and Super-Twisting Sliding Mode Control Techniques

Turki Alsuwian [1], Umar Riaz [2], Arslan Ahmed Amin [2,*], Muhammad Bilal Qadir [3], Saleh Almasabi [1] and Mohammed Jalalah [1,4]

1 Department of Electrical Engineering, College of Engineering, Najran University, Najran 11001, Saudi Arabia
2 Department of Electrical Engineering, FAST National University of Computer and Emerging Sciences, Chiniot Faisalabad Campus, Chiniot 35400, Pakistan
3 School of Engineering & Technology, National Textile University, Faisalabad 37610, Pakistan
4 Promising Centre for Sensors and Electronic Devices (PCSED), Advanced Materials and Nano-Research Centre, Najran University, Najran 11001, Saudi Arabia
* Correspondence: arslan.amin@nu.edu.pk; Tel.: +92-322-6259484

Abstract: Safety and critical applications employ fault-tolerant control systems (FTCS) to increase reliability and availability in the event of a failure of critical components. Process facilities may employ these technologies to cut down on production losses caused by equipment failures that occur on an irregular or unscheduled basis. Air–fuel ratio (AFR) adjustment in the fuel system of internal combustion engines (ICE) is crucial for enhancing engine efficiency, saving fuel energy, and safeguarding the environment. This paper proposes a novel hybrid fault-tolerant control system (HFTCS) for controlling the AFR in ICEs that combines the features of both an active fault-tolerant control system (AFTCS) and a passive fault-tolerant control system (PFTCS). The fault detection and isolation (FDI) unit is designed using fuzzy logic (FL) as part of an AFTCS to give estimated sensor values to the engine controller when the sensor becomes faulty. Super-twisting sliding mode control (ST-SMC) is implemented as part of a PFTCS to maintain AFR by adjusting the throttle actuator in the fuel supply line under faulty conditions. Lyapunov stability analysis is also performed to make sure that the system remains stable in both normal and faulty conditions. According to the results in the Matlab/Simulink environment, the suggested system stays robust and stable during sensor faults. In faulty situations, it also maintains the AFR at 14.6 without any degradation, and a comparison with previous studies is carried out. The study shows that the suggested approach is an innovative and highly dependable solution for AFR control in ICEs, preventing engine shutdown and output loss for higher profitability.

Keywords: air–fuel ratio control; IC engine; fault-tolerant control; fault detection and isolation unit; robust control; fuzzy logic control; super-twisting sliding mode control; analytical redundancy

Citation: Alsuwian, T.; Riaz, U.; Amin, A.A.; Qadir, M.B.; Almasabi, S.; Jalalah, M. Hybrid Fault-Tolerant Control for Air-Fuel Ratio Control System of Internal Combustion Engine Using Fuzzy Logic and Super-Twisting Sliding Mode Control Techniques. *Energies* **2022**, *15*, 7010. https://doi.org/10.3390/en15197010

Academic Editor: Theodoros Zannis

Received: 20 August 2022
Accepted: 20 September 2022
Published: 24 September 2022

1. Introduction

1.1. Air-Fuel Ratio (AFR) Control System

Internal combustion engines (ICEs) are utilized in the process industries for several prime mover applications, such as compressors and alternators. Depending on the combustion process, they are classified as compression ignition (CI) or spark ignition (SI). In SI ICEs, the air–fuel ratio (AFR) manages to stay within a narrow band around the stoichiometric value to meet strict engine exhaust emissions rules, as a rich or lean mixture reduces efficiency [1]. When an exact amount of fuel is provided for the combustion process as per the balanced chemical equation, the AFR of an ICE is referred to as the stoichiometric ratio. The AFR of an engine has an effect on several other characteristics of engine performance, including fuel consumption, combustion, and output torque [2]. As a result, AFR control has become a significant issue to eliminate dangerous engine emissions. All of the abbreviations used in the article are listed and a list of variables is provided in abbreviations.

The AFR system of an SI ICE is given in Figure 1. To eliminate dust particles, the air is blown through filters and is directed by a throttle valve. After the filtration fuel is injected into the engine manifold for the air–fuel mixture system, the flow of fuel is controlled by a fuel throttle actuator, which is then mixed with air and fed to the engine cylinders for combustion.

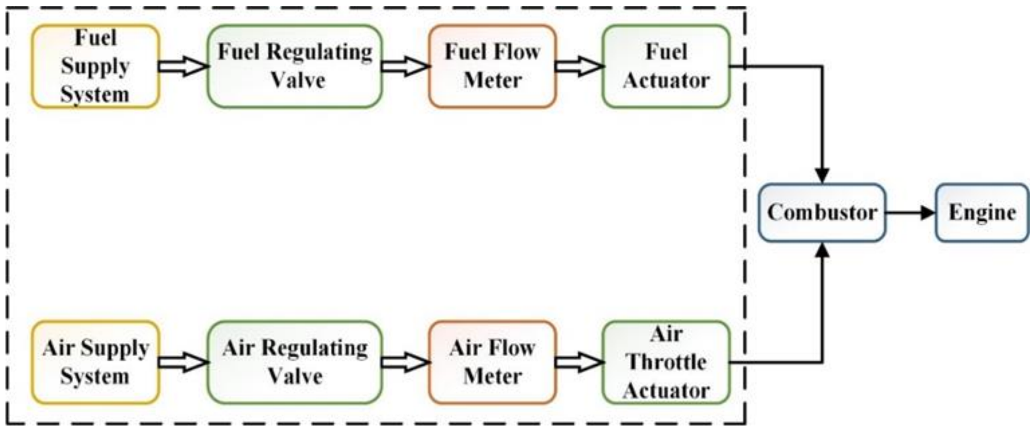

Figure 1. AFR System of SI ICE [2].

AFR is expressed mathematically as follows:

$$AFR = \frac{m_{air}}{m_{fuel}} \tag{1}$$

where m_{fuel} and m_{air} represent the respective masses of fuel and air. Following is a chemical equation that describes how gasoline fuel burns [3]:

$$25O_2 + 2C_8H_{18} \rightarrow 16CO_2 + 18H_2O + Energy \tag{2}$$

The AFR according to this equation is 14.6, which is also known as the stoichiometric ratio [3]. The AFR in gasoline combustion can vary from 6:1 to 20:1 according to mixture contents [4]. In this research, a gasoline engine was utilized to design an AFR controller for the ideal ratio of 14.6. In ICEs, the main aim is to keep this ratio constant for the best combustion results [5,6]. It also provides benefits such as decreased toxic emissions and fuel energy savings due to better engine efficiency [7,8].

Linear and non-linear control principles have been used to solve the problem of AFR control. As described in [9], Chen used estimation theory to manage the AFR of an IC engine. His study is focused on a single-cylinder engine, but it can be applied to multi-cylinder engines as well. Shiwei proposed a second-order sliding mode control for IC engine AFR control in his research as shown in [10]. In [11], fuzzy sliding mode control was proposed for a lean burn SI engine, which is model-free and does not need any system characteristics. In [12], a PI-like fuzzy knowledge-based controller for AFR control was proposed that is capable of self-tuning and is highly robust. In [13], the modeling for the AFR controller was performed in detail with stability proofs. For modeling uncertainties and lumped dynamics effects, the AFR control was used as a tracking control system and incorporated unknown input observers into the control system design as discussed in [14]. The famous mean value engine model was proposed in [15] for SI ICEs. The AFR control system is dependent on four important sensors [7], as shown below in Figure 2, and a short description is given.

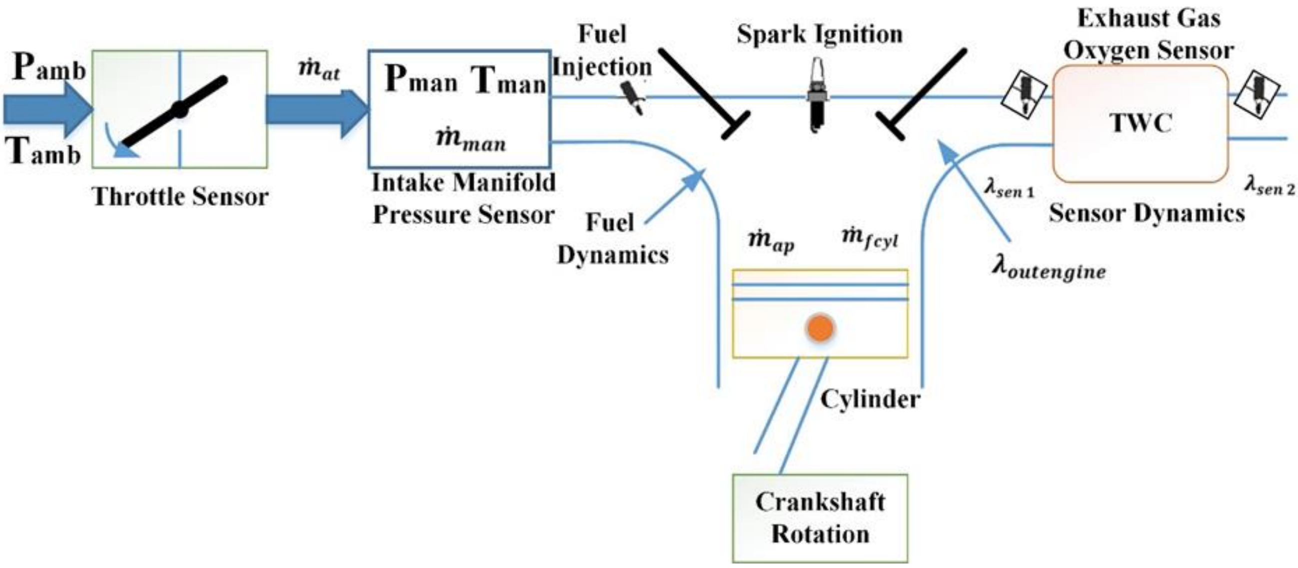

Figure 2. AFR system with Sensor Marking [16].

- ***Exhaust Gas Oxygen (EGO) Sensor:*** The percentage of oxygen in the engine exhaust gas is measured using an oxygen sensor. The input from the oxygen sensor is required to adjust the fuel mixture.
- ***Manifold Air Pressure (MAP) Sensor:*** The engine's electronic control unit receives immediate manifold pressure information from the manifold absolute pressure sensor.
- ***Throttle Sensor:*** The throttle valve's opening and closing actions are measured with a throttle sensor and communicated to an engine control module.
- ***Speed Sensor:*** This device is used to monitor the speed of the engine. It is utilized to communicate to the controller how fast the engine is moving.

The Engine Control Unit (ECU) contains an AFR controller that ensures an AFR of 14.6. When sensors and actuators fail due to undesired action, it produces unequal combustion and engine stoppage, resulting in increased engine unavailability for fault repair as well as a loss of power. The fault-tolerant control (FTC) concept is used to prevent the engine from shutting down, allowing it to continue to function normally during the faults.

1.2. Fault-Tolerant Control Systems

A fault is defined as a variation from the acceptable/normal state of system variables that might degrade the system performance. A system's normal functioning may vary from what is desired due to a failure, but this can be tolerated. Faults are considered to occur infrequently in systems, yet they cannot be prevented, as stated in [17–19]. Their implications, on the other hand, can sometimes be reduced by taking the right steps. As the name indicates, a fault-tolerant control system (FTCS) can tolerate faults while maintaining closed-loop performance, as shown in [20]. These techniques may also be used in different applications that require continuous servicing, including process industries, where it will help to increase profitability by preventing production losses as described in [21,22].

The FTCS is further divided into active FTCS (AFTCS) and passive FTCS (PFTCS) depending on how the problem is addressed. Hybrid FTCS (HFTCS) is designed with the help of both of these systems as stated in [23,24]. The fault detection and isolation (FDI) unit in the AFTCS delivers real-time information of system errors and failures. The observer concept is used in the FDI unit, and the algorithm provides a difference by comparing the system variable to a normal pre-determined value. Chetouani used an extended Kalman filter for FDI in nonlinear dynamical systems [25]. In residual-based FDI, inputs from a mathematical model and hardware observations are matched, and the filtered difference is exploited to provide a residual signal. The residuals should be zero in fault-free situations and nonzero when faults/failures occur. A fault is defined to occur when the residual signal exceeds the threshold, as discussed in [26]. Kobayashi and Simon in [27] highlighted the use of a bank of Kalman filters for evaluating aircraft engine faults.

The controller in a PFTCS has a fixed structure and does not require the FDI unit to provide up-to-date fault information. The objective of a PFTCS is to use robust control techniques to make the controller, but it can only handle faults that were considered during controller design. As stated in [28], PFTCS has been proposed using fuzzy logic control (FLC) for tank-level systems and a PI controller under system failures and process disturbances. For the air route of diesel engines, Murtaza reported a combined FDI and FTCS based on super-twisting control [29]. AFTCS, on the other hand, responds actively according to the FDI's faulty information. The AFTC system's structure is often more complex than the PFTCS, but it can handle a wider range of faults. Numerous methods have been used to implement AFTCS. In [30], Li and Tong used FLC for the adaptive control system to address the nonlinear parameters for actuator faults. Tang described how neural networks were applied in the average dwell approach in [31]. Carbot-Rojas described in a study [32] how a nonlinear adaptive observer was implemented in the FDI unit using real sensor values for flow rate estimation in a double pipe where heat is exchanged with an actuator fault. In [33], AFTCS was proposed for both sensor and actuator faults with the mathematical relationship of observers and redundant actuators for the anti-surge control system of centrifugal compressors.

HFTCS combines the two approaches to achieve the best solution for both uncertain and fixed problems. The HFTCS takes into account any faults in the running and designing stages. Because of this, the suggested approach becomes more reliable and efficient, which is why it is used in a variety of essential applications where human safety is essential. In [34], the HFTCS was suggested for the distillation column's sensors without using any intelligent control or data-driven method. The HFTCS was introduced in [35] for uncertain networked control systems using a discrete event-triggered communication mechanism that was not implemented in the process plant. In this research, we rely on analytical redundancy, and the software-based approach is utilized to generate parameter values in accordance with the existing model of the system, rather than utilizing extra hardware components. The control algorithm uses a software value in the case of a component fault.

1.3. Fuzzy Logic Control

FLC approaches are used to divide a complicated system into multiple subsystems based on human expertise. FLC is used in analyzing the effect of renewable energy sources in integrated energy water nexus planning in the presence of uncertainty, and a detailed review of its various application is given in [36,37]. The first stage in developing a control system is to make a mathematically based model of the system and the designed controller. The piecewise Lyapunov functions were used to create controllers for fuzzy dynamic systems in [38]. FLC applications in practical processes can be found everywhere; a brief study of a converter DC motor drive is given in [39]. In a comprehensive study on the intelligent AFR control strategy for gasoline direct-injection engines, a PI-like fuzzy knowledge-based controller was proposed [40]. The FLC design has two basic steps: the knowledge base design of FLC and its tuning.

The crisp output error time: error "e" and change in error "Δe" are firstly changed to fuzzy variables. The error signals are given as follows:

$$e_k = setpoint - output = SP - PV \tag{3}$$

$$\Delta e_k = e_k - e_{k-1} \tag{4}$$

The compositional rule of inference is used to examine the control rules, and the computed control action is then translated back to the crisp value, which is required to manage the process. For sensor faults in the AFR system of ICEs, FLC-based AFTCS was developed, as in [41], but this consisted only of the active part showing computational inefficiency.

1.4. Advanced Sliding Mode Control

Sliding mode control (SMC) is a kind of variable structure control with the properties of finite-time convergence, robustness, and reduced-order compensated dynamics. The SMC design is divided into two sections: the designing of a sliding surface and control law designing [42]. The sliding mode controllers with discontinuous high–frequency switching are intended to bring the sliding surface to zero. The system states in SMC are driven toward the sliding surface (SS). Figure 3 shows the graphical representation of SMC. After reaching SS, the SMC maintains the states in the near area of the SS. The SMC design is divided into two sections: SS and control law design.

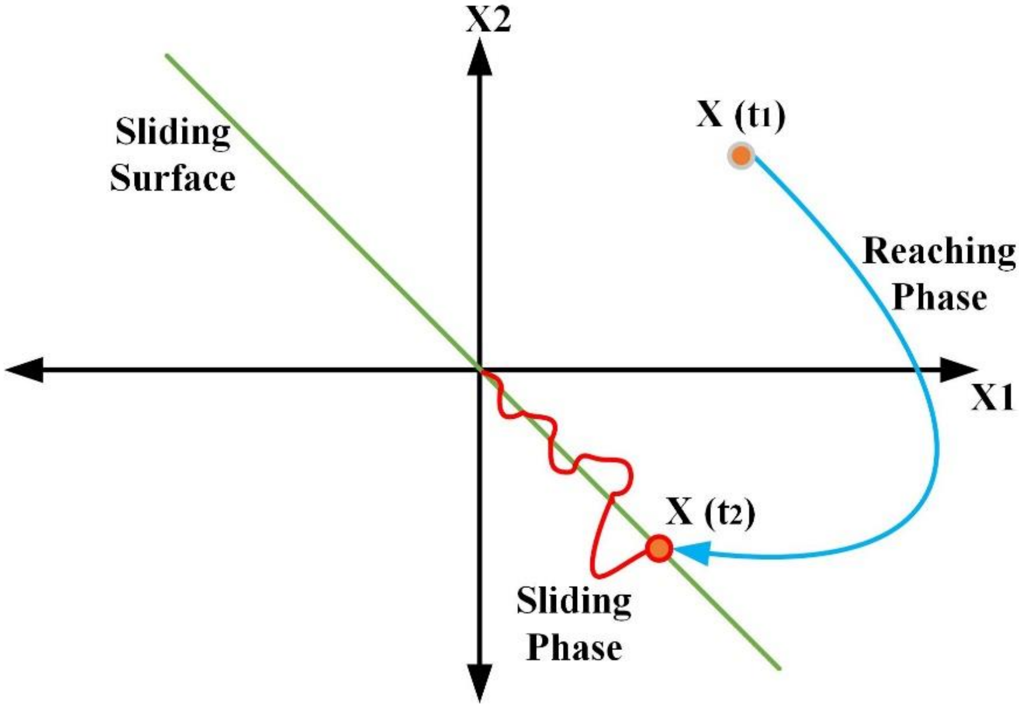

Figure 3. Graphical representation of SMC [42].

A sliding surface is given as follows:

$$\sigma = e^k + \sum_{i=0}^{k-1} c_i e^i \tag{5}$$

Here, $k = r - 1$ with r denoting the relative degree between u and y, and "c_i" is a positive constant that may be chosen at random. The value of σ should be chosen so that it equals 0 and produces a stable differential equation. The sliding surface design is given as follows for various values of k:

$$\left.\begin{array}{r} k = 1 \quad \sigma = \dot{e} + \lambda_e \\ k = 1 \quad \sigma = \ddot{e} + 2\lambda_{\dot{e}} + \lambda^2 e \end{array}\right\} \tag{6}$$

Control law design is the second step that should guide the variable to zero in a limited time, or should direct the system trajectories onto the sliding manifold. The discontinuous function "sgn" produces oscillation in many parts; applying the continuous functions "*sat*" and "*tanh*" reduces some chattering but does not preserve robustness.

The super-twisting sliding mode controller (ST-SMC) is an alternative to the standard first-order SMC, with a relative degree that does not degrade tracking performance or produce chattering. After specifying a trajectory similar to one of the twisting algorithms in [43], this technique converges the sliding variable in a finite duration with a suitable choice of parameters. The block diagram of ST-SMC is given in Figure 4.

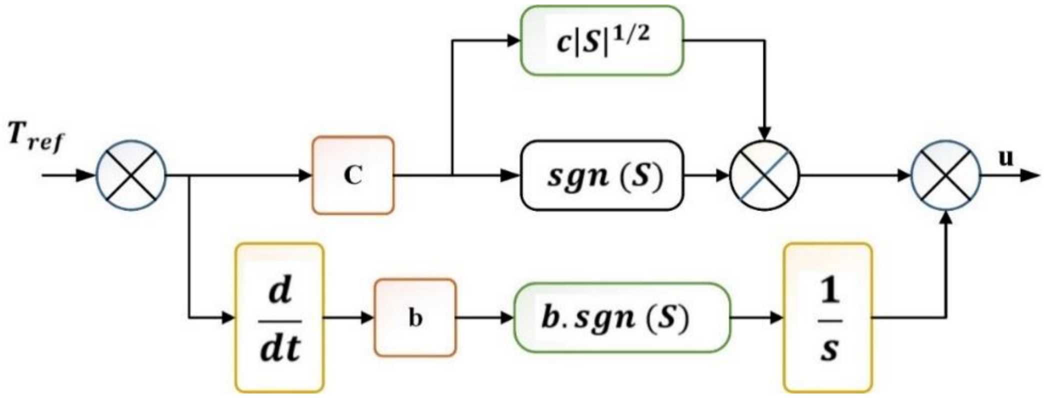

Figure 4. Block diagram of ST-SMC [43].

In Figure 3, "T_{ref}" is a reference value, "C" is constant, "b" is positive gain, "sgn" is signum function, and "u" is the output. The ST-SMC is well-suited to use since it is less sensitive to output measurement noise and potential faults in the calculation of σ as given in the research [44]. There are two terms in the ST-SMC control law $u(t)$. The discontinuous time derivative defines the first term, whereas the continuous function of the available sliding variable, which is only available during the reaching phase, defines the second [45]. The control law is described as:

$$\dot{u}_1(t) = \begin{cases} -u & if|u| > 1 \\ -Wsign(\sigma) & if|u| \leq 1 \end{cases} \tag{7}$$

$$u_2(t) = \begin{cases} -\lambda|\sigma_0|\rho sign(\sigma) & if|\sigma| > \sigma_0 \\ -\lambda|\sigma|\rho sign(\sigma) & if|\sigma| \leq \sigma_0 \end{cases} \tag{8}$$

Here, "σ_0" represents a boundary layer around the control value boundary, and "u" represents the control value boundary. The following are the required, as well as necessary and sufficient, requirements for finite time convergence to the sliding mode manifold:

$$\begin{gathered} W > \frac{\Phi}{\Gamma_m} \\ \lambda^2 \geq \frac{4\Phi\Gamma_{m\ (W+\Phi)}}{\Gamma_m^2\Gamma_m\ (W-\Phi)} \\ 0 < \rho < 0.5 \end{gathered} \tag{9}$$

W, ρ, λ are control gains, and Φ, W, Γ_M are positive constants. When controlled systems are linearly dependent on the control, $\sigma_0 = \infty$ and u do not need to be constrained. As a result, the controller's final equation may be reduced to:

$$\left.\begin{aligned} u(t) = -\lambda\sqrt{|\sigma|}sign(\sigma) + u_1 \\ \dot{u}_1(t) = -Wsign\ (\sigma) \end{aligned}\right\} \tag{10}$$

Here, $\lambda = \sqrt{u}$ and $W = 1.1u$ are used. U is a large-valued positive constant whose value is fine-tuned using the "trial and error" method till sufficient closed-loop performance is achieved. The control rule in Equation (10), which is used in the designing of the controller, is stable, and a step-by-step analysis of its stability is provided.

In this paper, our contribution is the development of an HFTCS for the reliability enhancement of the IC engine's AFR system. The proposed hybrid system includes AFTCS based on FLC for active compensation and PFTCS dependent on the ST-SMC controller for quick reaction to pre-defined faults of sensors. ST-SMC was implemented to maintain AFR by adjusting the throttle actuator in the fuel supply line under faulty conditions. Faults were introduced one by one to check the performance, and simulations were carried out in the MATLAB/Simulink environment. According to the results in the Matlab/Simulink environment, the suggested system stayed robust and stable during sensor faults. In faulty situations, it also maintains the AFR at 14.6 without any degradation, and a comparison with previous studies was also carried out to elaborate the benefits of the proposed HFTCS.

The following are the study's assumptions: (1) The engine works at a steady speed without regard to load changes. (2) In the event of faults, the sensors return to zero and the actuator shuts completely. The limitations of the research include the fact that it only examines the full-type failure of sensors and actuators and does not investigate partly faulty components. Another limitation is that this research only examines single sensor failures and not multiple sensor failures. The organization of the paper is as follows: Section 2 discusses the research methodology. Section 3 elaborates on the results and discussion. In Section 4, detailed comparisons with previous works are given. The last section, Section 5, covers the conclusion with a discussion of future research areas.

2. Research Methodology

The Matlab/Simulink model of the IC gasoline engine [46] was used for the development of the proposed HFTCS in which Mathworks describes an FTC system for an engine that uses four sensors and an air throttle that keeps the AFR at 14.6. In this model, the AFR system of the gasoline engine was built based on the findings of Crossley and Cook and was fully validated against dynamometer test data [47]. The mathematical equations used for the model construction were in accordance with the mean value engine model (MVEM) [15]. Moreover, it gives an accurate AFR as found in practical gasoline engines [1,2]. The FDI unit is designed to employ FLC-based observers to implement AFTCS. The PFTCS is designed with ST-SMC, which makes it robust against parameter changes caused by faults and noise. Since the engine in the process plant works at a constant speed most of the time, when the speed sensor fails, the 300 r/min is supplied to the controller by the newly designed FDI unit. By using Matlab model lookup tables (LTs), the required input data for the throttle and MAP sensors at a constant speed of 300 r/min was obtained. To generate a nonlinear relation between the MAP and throttle sensors, FLC methods were applied. For the estimation of faulty sensors' value, the FDI unit utilized these non-linear relationships. To test the controller's operation, a fault was manually injected one by one into all four sensors with the fault injection unit (FIU). The FLC observer produced a new estimated value based on the input data from the other active sensors, which was transmitted to the controller. The design of AFTCS, PFTCS, and HFTCS is further elaborated in the following subsections.

2.1. Modelling of AFR System

The three categories of AFR control dynamics are air dynamics, fuel dynamics, and sensor dynamics, as detailed in [2].

2.1.1. Dynamics of Air

The ideal air gas theory and conservation of mass can be used to describe the dynamics of the intake air.

$$\dot{P_{in}} = \frac{RT_{in}}{V_{in}}\left(\dot{m_{th}} - \dot{m_{Cyt}}\right) + P_{in}\frac{\dot{T_{in}}}{T_{in}} \quad (11)$$

$$\dot{P_{in}} = \psi(\varnothing_{th},\ P_{in},\ T_{in},\ N_e) \quad (12)$$

Here, P_{in} refers to the manifold pressure in the bar and T stands for the intake temperature in Kelvin. The mass flow into the valves is expressed by $\dot{m_{th}}$ (kg/s) and the mass flow into the cylinders is shown by and measured in (kg/s). The input volume is given by V_{in} and generally measured in (m^3). The general gas constant is given by R. The opening area (degree) of the throttle is measured in $\varnothing_{th}$ and the speed of the engine (rpm) is N_e. The temperature is assumed to be constant [15,46]. Therefore, the differential Equation (11) becomes at this point as follows:

$$\dot{P_{in}} = \dot{K_{in}}\left(\dot{m_{th}} - \dot{m_{Cyt}}\right) \quad (13)$$

$$\dot{K_{in}} = \frac{RT_{in}}{V_{in}} \tag{14}$$

The mass flow of air through the use of the valve is indicated as:

$$\dot{m_{th}} = C_d \frac{P_{id}}{\sqrt{RT_{id}}} S_{es}\ (\varnothing_{th}) g(P_r) \tag{15}$$

The discharge coefficient is represented by C_d. The variable P_{id} determines the excess loading pressure, and P_r is the load ratio determined by $P_r = \frac{P_{in}}{P_{id}} S_{es}\ (\varnothing_{th})$ is the throttle area, whereas the effective beginning throttle area is presented by $C_d S_{es}\ (\varnothing_{th})$. The symbol for this vector is:

$$S_{ett}(\varnothing_{th}) = C_d S_{es}(\varnothing_{th}) = \sigma_1\{1 - \cos(\sigma_2 \varnothing_{th} + \sigma_3)\} + \sigma_4 \tag{16}$$

Here, $g(P_r)$ is a non-linear concept in the sense that:

$$g(P_r) = \begin{cases} \sqrt{\frac{2\gamma}{\gamma-1}} (P_r)^{\frac{1}{\gamma}} \sqrt{\left(1 - P_r^{\frac{\gamma-1}{\gamma}}\right)} if P_r > \left(\frac{2}{\gamma+1}\right)^{\frac{\gamma}{\gamma-1}} \\ \sqrt{\gamma} \left(\frac{2}{\gamma+1}\right)^{\frac{\gamma+1}{2\ (\gamma-1)}} if P_r \leq \left(\frac{2}{\gamma+1}\right)^{\frac{\gamma}{\gamma-1}} \end{cases} \tag{17}$$

where γ is the specific heat ratio of air and normally its value is usually taken as 1.4.

2.1.2. Dynamics of Fuel

The dynamics for fuel are elaborated as follows:

$$\begin{cases} \ddot{m}_{ff}(t) = \frac{1}{\tau_f}\left(-\dot{m}_{ff}(t) + x\dot{m}_{ft}(t)\right) \\ \dot{m}_{fv} = (1-x)\dot{m}_{fv}(t) \\ \dot{m}_f(t) = \dot{m}_{fv}(t) + \dot{m}_{ff}(t) \end{cases} \tag{18}$$

Based on the engine's rpm, it might be utilized as a vector, "Ne", to attain a more complete analysis. Where "$\tau_{f''}$ is the fuel vapor phase at the time (s), "$\dot{m}_{fi}(t)$" is the fuel flow injection (kg/s), "$\dot{m}_f(t)$" is the fuel flow into the cylinders (kg/s), and "$\ddot{m}_f(t)$" is the vapor fuel flow (kg/s). Consider "x" as a variable that depends on the throttle opening or engine speed to get a more accurate model

$$\tau_f(N_e) = \sigma_5 N_e^{-\sigma_6} \tag{19}$$

$$x(N_e) = \sigma_7 + \sigma_8 N_e \tag{20}$$

where σ_5, σ_6, σ_7, σ_8 are constant parameters. The injector model is given by a linear relationship between the mass fuel flows from the injectors. AFR can now be obtained as follows:

$$\lambda_{cyl} = \frac{\dot{m}_{cyl\ (t)}}{\lambda_s \dot{m}_{f(t)}} \tag{21}$$

2.1.3. Sensor Model

The sensor model is given as follows:

$$\dot{\lambda}(t) = -\frac{1}{\tau_\lambda}\lambda(t) + \frac{1}{\tau_\lambda}\lambda_{cyl}(t - \tau(N_e(t))) \tag{22}$$

and the constant delay is $\tau_\lambda = 0.1\ Sec$.

Engine speed *Ne(t)* is expressed in Equation (23) with a delay time.

$$\tau(N_e(t)) = \frac{60}{N_e(t)}\left(1 + \frac{1}{n_{cyl}}\right) \tag{23}$$

2.1.4. State Space Representation

The following is a description of how the model is represented in state space:

$$\begin{bmatrix} \dot{x}_1 \\ \dot{x}_2 \end{bmatrix} = A\begin{bmatrix} x_1 \\ x_2 \end{bmatrix} + B\begin{bmatrix} u_1 \\ u_2 \end{bmatrix} \tag{24}$$

$$y = C\begin{bmatrix} x_1 \\ x_2 \end{bmatrix} + D\begin{bmatrix} u_1 \\ u_2 \end{bmatrix} \tag{25}$$

$$\begin{cases} \dot{x}_1 = f_1(.)x_1(t) - f_2(.)u(t) \\ \dot{x}_2 = -\frac{1}{\tau_\lambda}\lambda(t) + \frac{1}{\tau_\lambda}\lambda_{cyl}(t - \tau(N_e(t))) \end{cases} \tag{26}$$

with $x_1(t) = \lambda_{cyl}, x_2(t) = \lambda(t)$ and $u(t) = \dot{m}_{fi}(t)$

$$f_1(.) = -\frac{1}{\tau_\lambda(N_e)} - \frac{\ddot{m}_{cyl}}{m_{cyl}(N_e,\ P_{in})} \tag{27}$$

$$f_2(.) = \lambda_s \frac{\chi(N_e)}{\tau_f(N_e)}\, m_{cyl}(N_e,\ P_{in}) \tag{28}$$

bounded as follows: $f_{-i} \leq f_i(.) \leq \overline{f}_i for\ i \in \{1,\ 2\}$.

2.2. Design of AFTCS

To explain the AFTCS observer architecture suggested by Wang in [21], the working flow chart of AFTCS is given in Figure 5. In state-space, the process can be modeled as follows:

$$\dot{x} = Ax + Bu \tag{29}$$

$$y = Cx + Du \tag{30}$$

In the above equations, states of the system are represented by "x", input is denoted by "u", and output of the system is represented by "y". The matrices of the system are shown by (A, B, C, D), respectively. Assume $\overline{x}$ indicates the estimated value produced by the system. As a result, the observer model is:

$$\dot{\overline{x}} = A\overline{x} + Bu \tag{31}$$

$$\overline{y} = C\overline{x} \tag{32}$$

$$\left(\dot{\overline{x}} - \dot{x}\right) = A\ (\overline{x} - x) \tag{33}$$

where $\overline{x} - x = e_x$ represents a difference between the system's actual and expected output, and:

$$(\ \overline{y} - y\ ) = C\ (\overline{x} - x) \tag{34}$$

$$\dot{\overline{x}} = A\overline{x} + Bu + L\ (\ \overline{y} - y\Big) \tag{35}$$

Feedback gain is given by L

$$\left(\dot{\overline{x}} - \dot{x}\right) = A\ (\overline{x} - x) + L\ (\ \overline{y} - y) \tag{36}$$

$$(\ \overline{y} - y\ ) = C\ (\overline{x} - x) \tag{37}$$

$$\left(\dot{\overline{x}} - \dot{x}\right) = (A + LC)\ (\overline{x} - x) \tag{38}$$

$$\dot{e}_x = (A + LC)e_x \tag{39}$$

$$(\overline{y} - y) = Ce_x \tag{40}$$

The FDI unit will not detect a fault until the residual "e_x" tends to zero. If the residual (difference) exceeds a certain set point, then the fault is recognized and the FDI unit is utilized to replace the incorrect value with the newly generated estimated value, which is obtained from an observer. When there is no issue in the system, it operates normally; nonetheless, when a single sensor in the system fails, the FLC-based observer gives the ECU an estimated value.

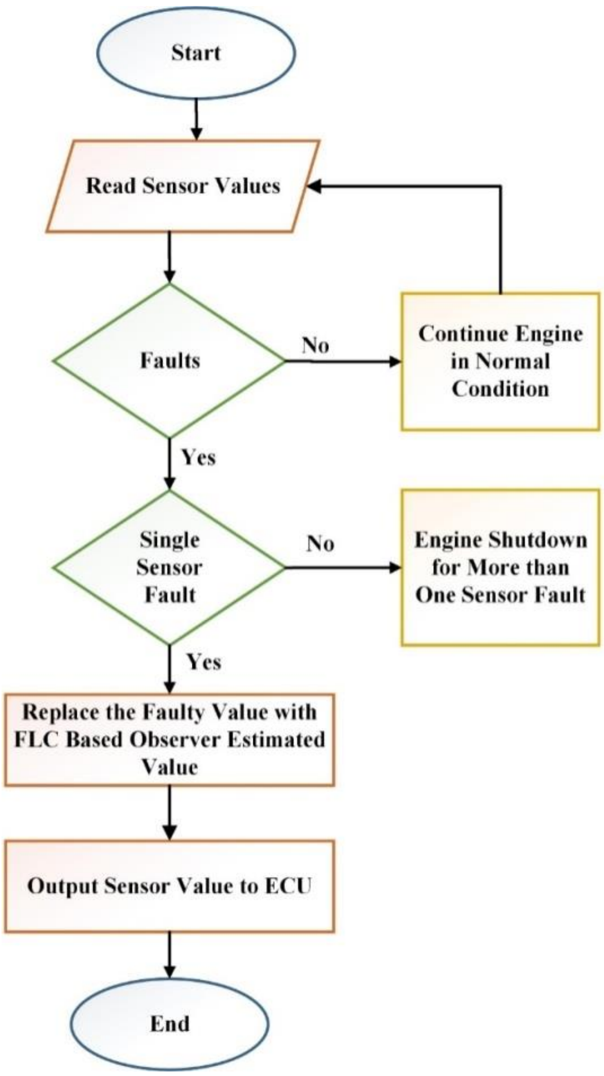

Figure 5. Flowchart of proposed AFTCS.

When the MAP sensor fails, the throttle sensor provides estimation, and when the throttle sensor fails, the MAP sensor provides estimation. As a result, the system operates smoothly in both faulty and normal settings.

AFTCSs are constructed utilizing state-space modeling to lessen the effects of these defects. Detailed research shows the state-space representation of the ICE [13]:

$$y = u + \alpha x_1 + \beta x_2 \tag{41}$$

$$u = y_d + \alpha x_1 + \beta x_2 \tag{42}$$

$$x_1 = f_1(.)x_1 - f_2(.)u(t) \tag{43}$$

$$x_2 = -\frac{1}{\tau_\lambda}\lambda(t) + \frac{1}{\tau_\lambda}\lambda_{cyl}(t - \tau(N_e(t))) \tag{44}$$

Here, x_1 and x_2 represent system states, while u, y, and y_d denote the system's inputs, real outputs, and desired output of the system. The engine parameter is represented by α and β, which are used to calculate the speed of the engine, N_e.

$$u = y_d + \alpha\overline{x}_1 + \beta\overline{x}_2 \tag{45}$$

The variables of this FLC-based observer are calculated using a gradient descent approach. The mean square error (MSE) is used to develop an observer that can reliably predict the exact output value. The MSE is given below.

$$E = \frac{1}{2}(y - \overline{y})^2 \tag{46}$$

In the above equation, the estimated output is given as $\overline{y}$ and the actual output of the system is represented by "y". The MSE is represented by E. The following would be the predicted output performance of the system:

$$\overline{y} = u + \alpha\overline{x}_1 + \beta\overline{x}_2 \tag{47}$$

In a steady-state system, the required production, y_d, must correspond with the predicted output. The conclusion is:

$$E = \frac{1}{2}(y - y_d)^2 \tag{48}$$

The error function is explained by the above equations, and a partial derivative of it is given as:

$$\frac{\partial E}{\partial x_1} = -\alpha(y - y_d) \tag{49}$$

$$\frac{\partial E}{\partial x_2} = -\beta(y - y_d) \tag{50}$$

The state variables are further modified as:

$$\overline{x}_1(k+1) = \overline{x}_1(k) - \eta\frac{\partial E}{\partial x_1} \tag{51}$$

$$\overline{x}_2(k+1) = \overline{x}_2(k) - \eta\frac{\partial E}{\partial x_2} \tag{52}$$

Both $\overline{x}_1$ and $\overline{x}_2$ denote expected values, (k) and $(k+1)$ represent intervals, and the learning rate is denoted by η. This is obtained by putting the values of Equations (49) and (50) into Equations (51) and (52).

$$\overline{x}_1(k+1) = \overline{x}_1(k) + \eta\alpha(y - y_d) \tag{53}$$

$$\overline{x}_2(k+1) = \overline{x}_2(k) + \eta\beta(y - y_d) \tag{54}$$

$$\eta = \frac{1}{\alpha^2 + \beta^2} \tag{55}$$

Here, the stability is higher, the learning rates are much lower, the settling time is reduced, and the percentage overshoot is relatively low. We achieved the following by using the value η of in Equations (53) and (54):

$$\overline{x}_1(k+1) = \overline{x}_1(k) + \frac{\alpha}{\alpha^2 + \beta^2}(y - y_d) \tag{56}$$

$$\overline{x}_2(k+1) = \overline{x}_2(k) + \frac{\beta}{\alpha^2 + \beta^2}(y - y_d) \tag{57}$$

We performed the Lyapunov proof to verify the stability of the controller and confirmed that it operates as intended, as briefly discussed in [13]. The dependability of the control system must be guaranteed for proper functioning. To show the system's stability, this FLC-based control technique uses a direct Lyapunov technique. The Lyapunov function is given as:

$$V(x(k)) = (y_d - y)^2 \tag{58}$$

Here, $V(x(k))$ should equal zero if the actual output matches the expected output. The actual and desired output values entered into the Lyapunov function are as follows:

$$V(x(k)) = [\alpha(x_1(k)) - \overline{x}_1(k) + \beta(x_2(k)) - \overline{x}_2(k)] \tag{59}$$

The state prediction faults are illustrated below, and we obtained this after solving the above equation:

$$\widetilde{x}_1(k) = (x_1(k) - \overline{x}_1(k)) \tag{60}$$

$$\widetilde{x}_2(k) = (x_2(k) - \overline{x}_2(k)) \tag{61}$$

Now the Lyapunov function becomes:

$$V(x(k)) = [\alpha\widetilde{x}_1(k) + \beta\widetilde{x}_2(k)] \tag{62}$$

By shifting the cycle (k) into the $(k+1)$ cycle, we obtained the following result:

$$V(x(k+1)) = [\alpha\widetilde{x}_1(k+1) + \beta\widetilde{x}_2(k+1)] \tag{63}$$

Here:

$$\widetilde{x}_1(k+1) = (x_1(k+1) - \overline{x}_1(k+1)) \tag{64}$$

$$\widetilde{x}_2(k+1) = (x_2(k+1) - \overline{x}_2(k+1)) \tag{65}$$

We obtained the following result by entering the value of Equations (56) and (57) into Equations (64) and (65):

$$\widetilde{x}_1(k+1) = x_1(k+1) - \overline{x}_1(k) - \eta\frac{\alpha}{\alpha^2 + \beta^2}(y - y_d) \tag{66}$$

$$\widetilde{x}_2(k+1) = x_2(k+1) - \overline{x}_2(k) - \eta\frac{\beta}{\alpha^2 + \beta^2}(y - y_d) \tag{67}$$

With the variation between actual and desired output, we obtained the following:

$$y - y_d = \alpha(x_1(k) - \overline{x}_1(k)) + \beta(x_2(k) - \overline{x}_2(k)) \tag{68}$$

By entering the value of Equations (60) and (61) into Equation (68):

$$y - y_d = \alpha\widetilde{x}_1(k) + \beta\widetilde{x}_2(k) \tag{69}$$

By entering the values from difference Equation (69) into Equation (66):

$$\overline{x}_1(k+1) = x_1(k+1) - \overline{x}_1(k) - \frac{\alpha}{\alpha^2 + \beta^2}[\alpha\widetilde{x}_1(k) + \beta\widetilde{x}_2(k)] \tag{70}$$

$$\overline{x}_2(k+1) = x_2(k+1) - \overline{x}_2(k) - \frac{\beta}{\alpha^2 + \beta^2}[\alpha\widetilde{x}_1(k) + \beta\widetilde{x}_2(k)] \tag{71}$$

As we previously discussed:

$$x_1(k+1) = x_1(k) \tag{72}$$

$$x_2(k+1) = x_2(k) \tag{73}$$

$$\overline{x}_1(k+1) = x_1(k) - \overline{x}_1(k) - \frac{\alpha}{\alpha^2+\beta^2}[\alpha\widetilde{x}_1(k) + \beta\widetilde{x}_2(k)] \tag{74}$$

$$\overline{x}_2(k+1) = x_2(k) - \overline{x}_2(k) - \frac{\beta}{\alpha^2+\beta^2}[\alpha\widetilde{x}_1(k) + \beta\widetilde{x}_2(k)] \tag{75}$$

Using Equations (60) and (61) as inputs, the values of Equations (74) and (75) become:

$$\overline{x}_1(k+1) = \widetilde{x}_1(k) - \frac{\alpha}{\alpha^2+\beta^2}[\alpha\widetilde{x}_1(k) + \beta\widetilde{x}_2(k)] \tag{76}$$

$$\overline{x}_2(k+1) = \widetilde{x}_2(k) - \frac{\beta}{\alpha^2+\beta^2}[\alpha\widetilde{x}_1(k) + \beta\widetilde{x}_2(k)] \tag{77}$$

The Lyapunov function is denoted as:

$$V(x(k+1)) = \begin{bmatrix} \alpha\left[\widetilde{x}_1(k) - \frac{\alpha}{\alpha^2+\beta^2}[\alpha\widetilde{x}_1(k) + \beta\widetilde{x}_2(k)]\right] \\ +\beta\left[\widetilde{x}_2(k) - \frac{\beta}{\alpha^2+\beta^2}[\alpha\widetilde{x}_1(k) + \beta\widetilde{x}_2(k)]\right] \end{bmatrix} \tag{78}$$

After solving, we achieved the following result:

$$V(x(k+1)) = 0 \tag{79}$$

Thus, the variance between both the (k) and (k + 1) cycles of the Lyapunov function is:

$$V(x(k+1)) - V(x(k)) = -(y_d - y)^2 \tag{80}$$

$\therefore V(x(k)) = (y_d - y)^2$ By entering this value into the above Equation (80), as given in Equation (50):

$$V(x(k+1)) - V(x(k)) = -V(x(k)) \tag{81}$$

Since $V(x(k)) = \dot{V}(x(k))$:

$$V(x(k+1)) - V(x(k)) = \dot{V}(x(k)) \tag{82}$$

This indicates that the variance between the Lyapunov function's cycles "k" and "(k + 1)" is negative-definite. Next, we developed the observer design equation for a nonlinear control system.

$$\widetilde{x}_1(k) = A\overline{x} + Bu + g(\overline{x},\ u,\ k) + \overline{L}(C\overline{x} - y) \tag{83}$$

Here, "g" is known as a function, which is the nonlinear observer's feedback gain. Assuming the error is:

$$e_x(k) \triangleq \overline{x}(k) - x(k) \tag{84}$$

The error equation becomes, for a nonlinear observer:

$$\dot{e}_x = \left(A + \overline{L}C\right)e_x(k) + \left(g(\overline{x},\ u,\ k) - g(x,\ u,\ k)\right) \tag{85}$$

Whenever there is a matrix and a scalar that meet a given linear matrix inequality, the error asymptotically goes to zero:

$$\begin{bmatrix} RA + A^T R + XC + C^T X^T + \mu\lambda^2 I & R \\ R & -\mu I \end{bmatrix} < 0 \tag{86}$$

where "R" stands for the reliability of the sensor. The following criteria are used to select the observer gain matrix:

$$\overline{L} = R^{-1}X \tag{87}$$

Consider the following to demonstrate that the Lyapunov function's derivative is zero:

$$V(k) = e_x^T R e_x(k) \tag{88}$$

Next, we observed $\dot{V}(x) < 0 \forall x \in D - \{0\}$ as stated below:

$$\begin{aligned}
\dot{V}(k) \; &= e_x^T \left(RA + R\overline{L}C + A^T R + C^T L^{-T} R\right) e_x \\
&+2e_x^T R(g(\overline{x},\, u,\, k) - g(x,\, u,\, k)) \leq e_x^T \\
&\times \left(RA + R\overline{L}C + A^T R + C^T L^{-T} R\right) e_x \\
&+ \tfrac{1}{\mu e_x^T R^2 e_x} + \mu \parallel g(\overline{x},\, u,\, k) - g(x_1,\, u,\, k) \parallel^2 \\
&\leq e_x^T \left(RA + R\overline{L}C + A^T R + C^T L^{-T} R\right) e_x \\
&+ \tfrac{1}{\mu e_x^T R^2 e_x} + \mu\lambda^2 \parallel e_x \parallel^2 \\
&= e_x^T \left(\left(RA + R\overline{L}C + A^T R + C^T L^{-T} R\right) + \mu\lambda^2 I + 1/\mu R^2\right) e_x
\end{aligned} \tag{89}$$

The following conclusions are obtained when the observer gain equation is incorporated into the previous equation:

$$\dot{V}(x) \leq e_x^T \left(\left(RA + R\overline{L}C + A^T R + C^T L^{-T} R\right) + \mu\lambda^2 I + 1/\mu R^2\right) e_x \tag{90}$$

e_x approaches zero if the following inequality somehow holds.

$$\left(\left(RA + R\overline{L}C + A^T R + C^T L^{-T} R\right) + \mu\lambda^2 I + 1/\mu R^2\right) < 0 \tag{91}$$

From the equations, we conclude that proof is achieved.

2.3. Design of PFTCS

In the fuel supply line, a fuel actuator is introduced. This fuel actuator is controlled by an ST-SMC-based controller [43] with a set point of 14.6. The control command from this controller is received by the fuel actuator. For the design of the PFTCS, the estimate blocks of the original model were removed. The flowchart of the proposed PFTCS is given in Figure 6.

The output tracking is defined as:

$$e = y_c\,(t) - y(t) \tag{92}$$

Here, "e" represents output tracking error,"$y_c\,(t)$" indicates reference value, and "$y(t)$" shows feedback.

The sliding surface is designed as:

$$\sigma = \dot{e} + ce \tag{93}$$

Here, "σ" is the sliding surface, "$\dot{e}$" indicates derivative of error, c represents constant time, and "e" is the error itself.

Where $c > 0$, the continuous control law brings the "sliding variable" to zero with finite time.

$$u = c\,|\sigma|^{1/2}\,sign\,(\sigma) + w \tag{94}$$

$$\dot{w} = b\,sign\,(\sigma) \tag{95}$$

As has been established, ST-SMC is continuous, because both:

$$c\,|\sigma|^{1/2}\,sign\,(\sigma) \tag{96}$$

and:

$$w = \int b\ sign\ (\sigma)dt \tag{97}$$

The controller, "u", that brings the sliding variable to zero in a finite time is given as:

$$u = -\rho\ sign\ (\sigma) \tag{98}$$

$$u = -sign\left(x_2 + c|x_1|^{\frac{1}{2}}\ sign\ (x_1)\right) \tag{99}$$

Here, "ρ"*is* the positive gain and sufficiently large.

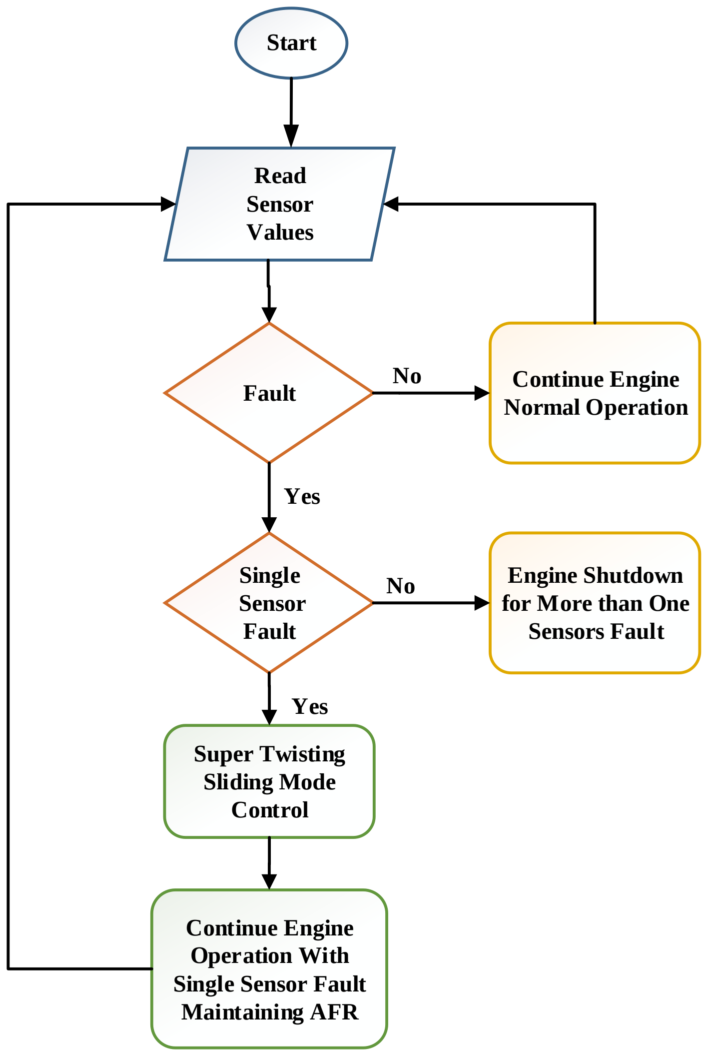

Figure 6. Flowchart of the proposed PFTCS.

2.4. Design of HFTCS

Both the FDI unit and robust control were utilized in the design of the HFTCS. When a sensor fails, the FDI unit calculates the estimated value of that sensor with the help of other healthy sensors. When the AFR value declines from 14.6 to 11.7 due to sensor fault, then the ST-SMC acts as a robust controller to keep the AFR value at 14.6. The proposed HFTCS flowchart is given in Figure 7.

The important parameters used in the model are mentioned in Table 1.

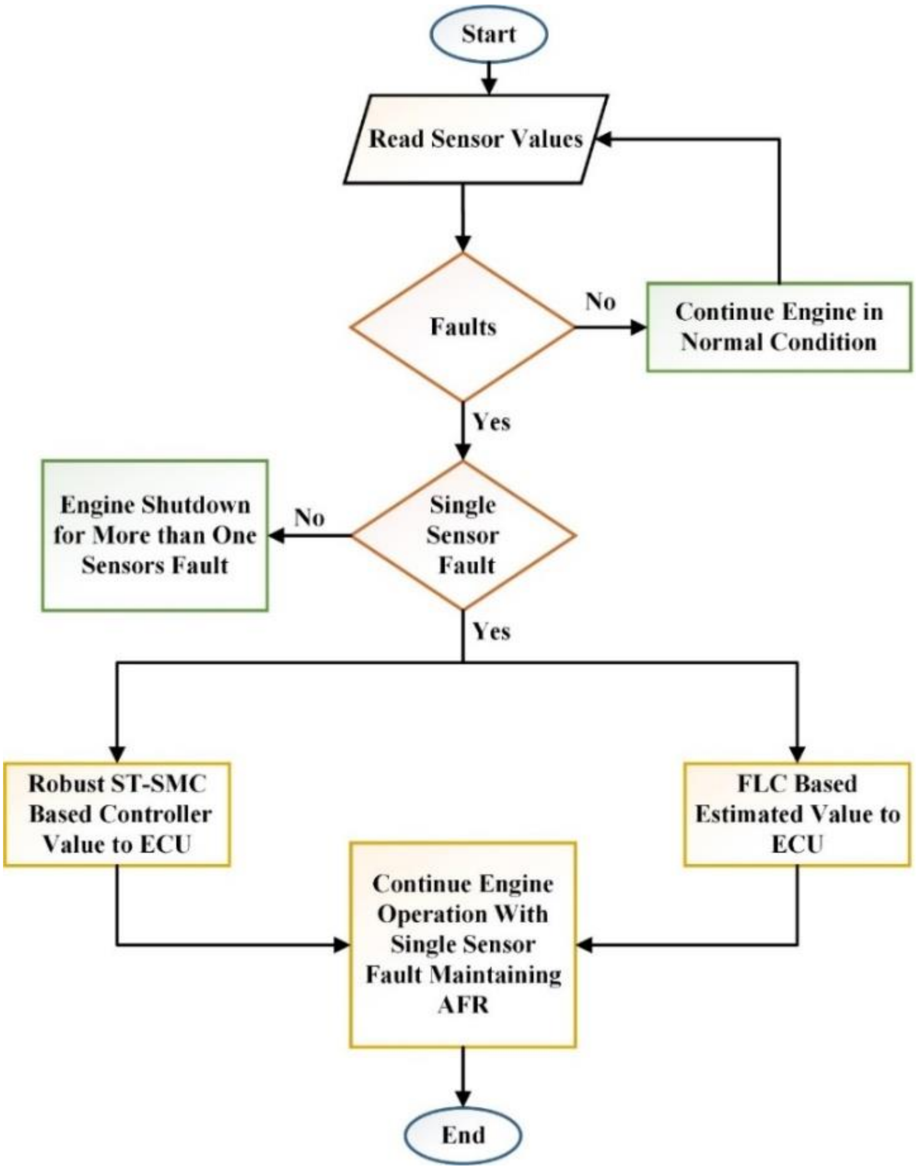

Figure 7. Flowchart for proposed HFTCS.

Table 1. Model Parameters [46,47].

Parameters	Values
Engine Speed	0–1000 rpm (300 rpm used in this study)
Throttle Sensor Range	0–90 degrees
MAP Sensor Range	0–1 bara
EGO Sensor Range	0–1 volts
Specific heat ratio, γ	1.414

3. Results and Discussion

The Matlab design for the suggested AFTCS components is shown in Figure 8. The FLC-based observer model was used as an FDI unit to estimate MAP and throttle values. MAP, EGO, throttle, and speed sensors are all included in this model.

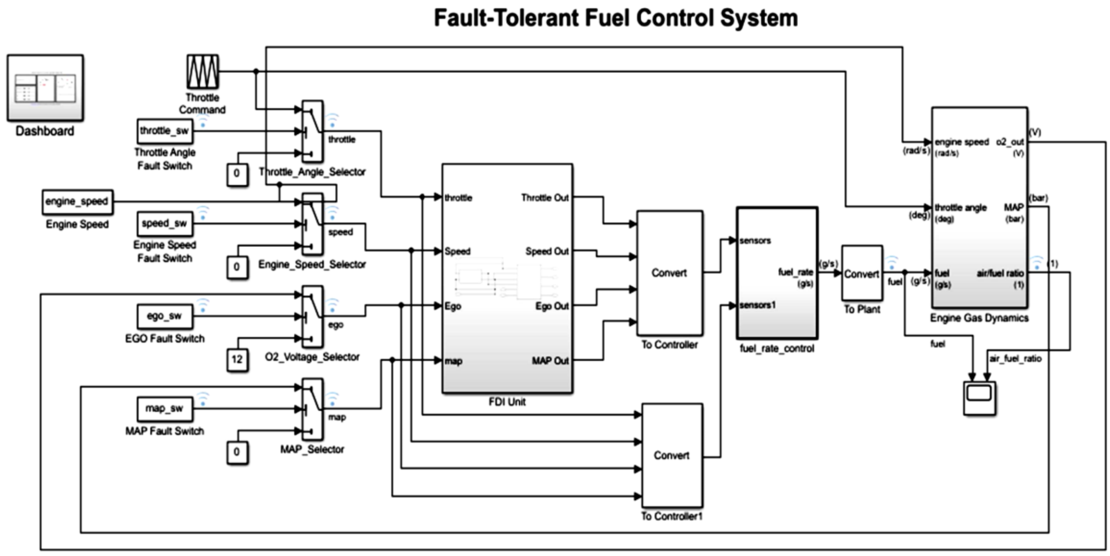

Figure 8. Matlab diagram of proposed AFTCS.

In the case of a sensor failure, the FDI estimation unit calculates the throttle and MAP values. The reconfiguration block creates the output based on the estimation of the FLC-based estimation unit, which is subsequently delivered to the ECU. When a value exceeds a certain threshold, the system detects a fault, and then the faulty value is updated with the FLC-based observer's estimated value. For this simulation, the fuzzy interference system (FIS) editor is utilized, and for the transformation of input into output, "if...then" rules are used. The FLC's response is calculated in Matlab/Simulink. In our research, to compute the throttle valve estimated value, the value of the MAP sensor was used as an input; similarly, to calculate the MAP value, the throttle sensor value was utilized as an input.

There were a total of 28 rules made for MAP estimation, and 19 rules built for throttle estimation, by using the (LTs) sensor data. The MAP input and throttles output membership functions (MFs) are shown in Figure 9. The MFs for throttle input and MAP output are given in Figure 10. The analysis for throttle estimation and MAP estimation is given in Figure 11. We selected triangle MFs because they provide a quick solution to the optimization problems that arise in fuzzy modeling. Straight lines are used to create the triangular MFs and these are easily editable. These straight-line MFs have the benefit of being simple to define and need a small amount of data.

The fault was injected into each sensor one by one with the FIU while the others sensors remained healthy. Because of the engine's internal warm-up time, its response was noticed at a time of 5 s. This result, given in Figure 12, shows that AFR was initially affected, but it quickly maintained the required ratio due to the FLC-based observer's estimated value. In normal conditions, the AFR stays at 14.6 and decreases to 11.7 under faulty conditions. However, despite decreased performance in faulty situations, the system's stability is guaranteed, fulfilling the goal of fault tolerance.

The Matlab diagram for the PFTCS part is represented in Figure 13. An additional fuel actuator was added to the fuel supply line in this PFTCS design. This fuel actuator takes the output value of the ST-SMC controller as well as the fuel output, and the output of this actuator is sent to the ECU.

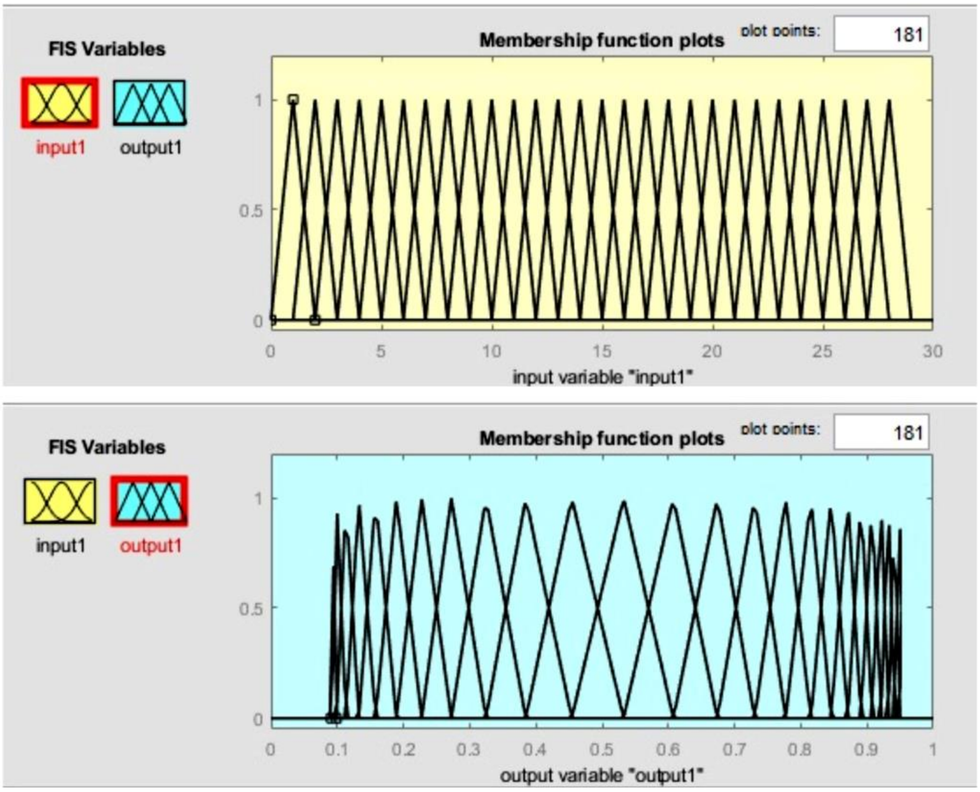

Figure 9. MFs for MAP input and throttle output.

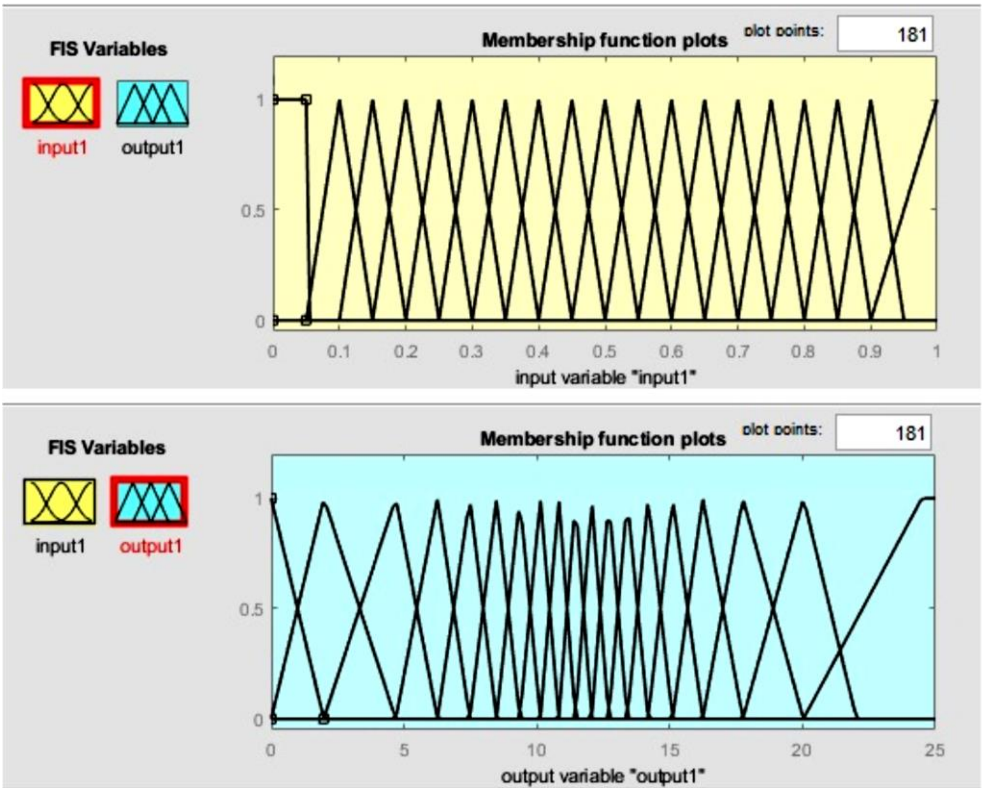

Figure 10. MFs for throttle input and MAP output.

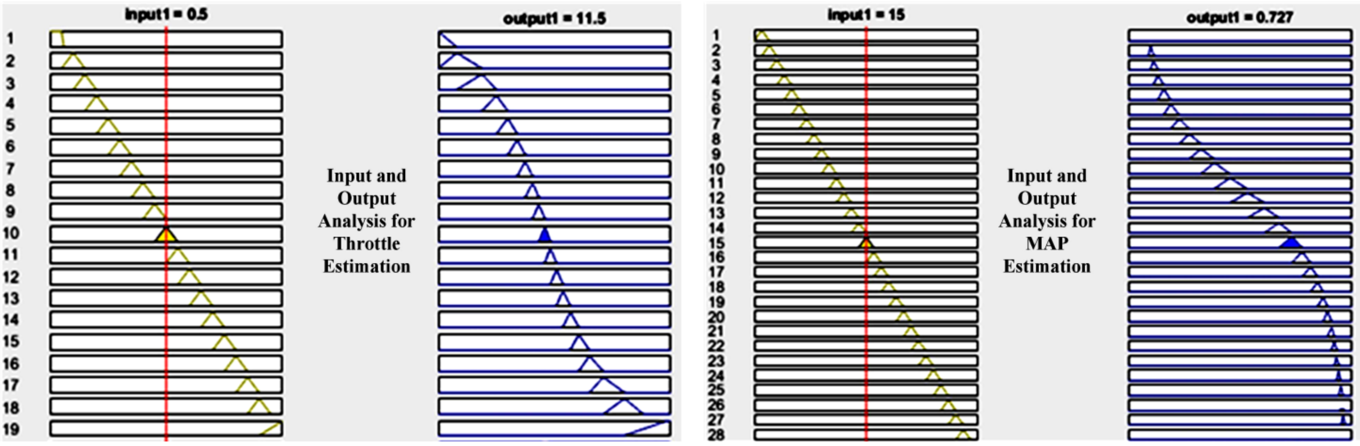

Figure 11. Input and output analysis for MAP and throttle estimation.

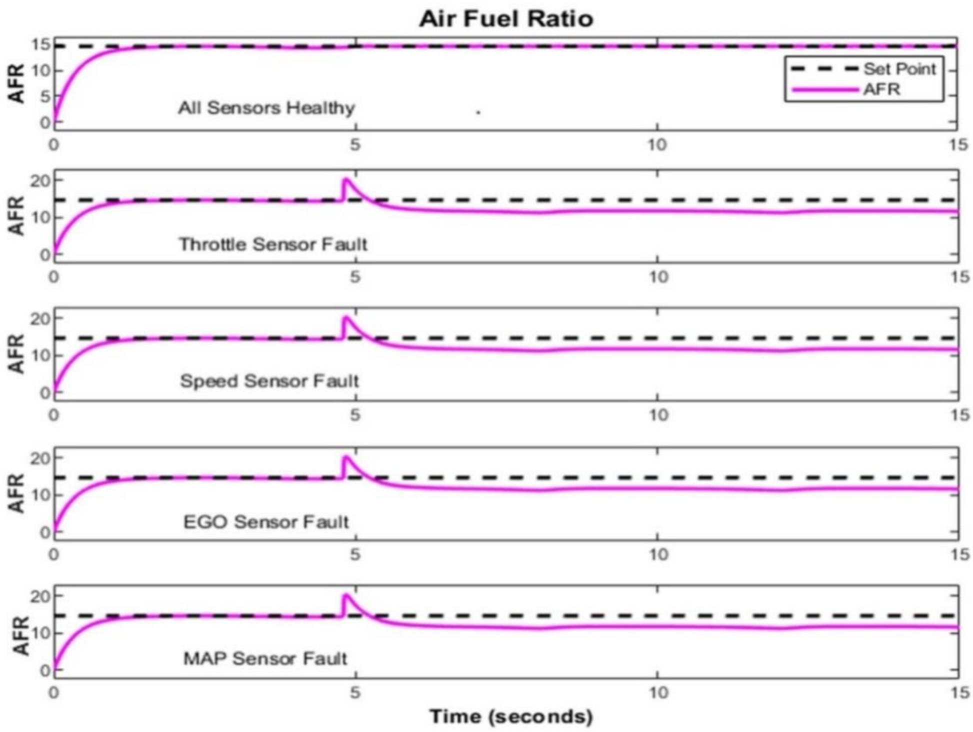

Figure 12. Performance of AFTCS.

The fault switch on this actuator is linked to the system's dashboard. When a fault is inserted into this actuator, the fuel flow to the engine is stopped.

The performance of the PFTCS in the case of a single sensor fault is shown in Figure 14. This graph indicates that the system's behavior was reliable and did not deviate from 14.6 in faulty situations.

These oscillations are generated by an SMC's high-frequency switching, which excites unmolded dynamics in the closed system. 'Unmolded dynamics' might be those of sensors and actuators which were neglected during the main modeling, since they are often much faster than the main system dynamics.

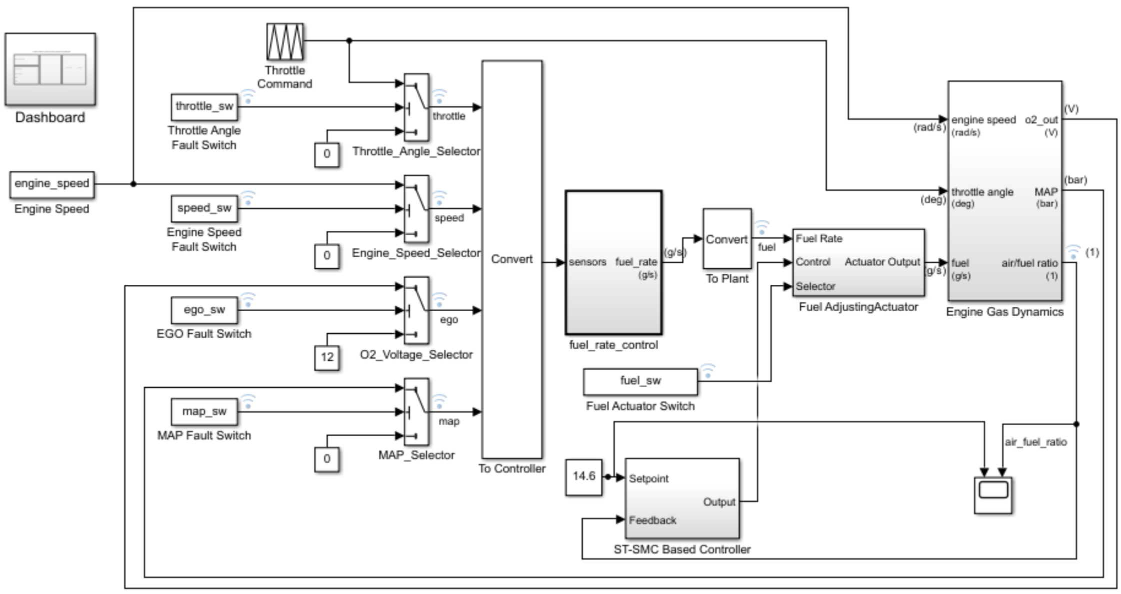

Figure 13. Matlab Diagram for PFTCS Part.

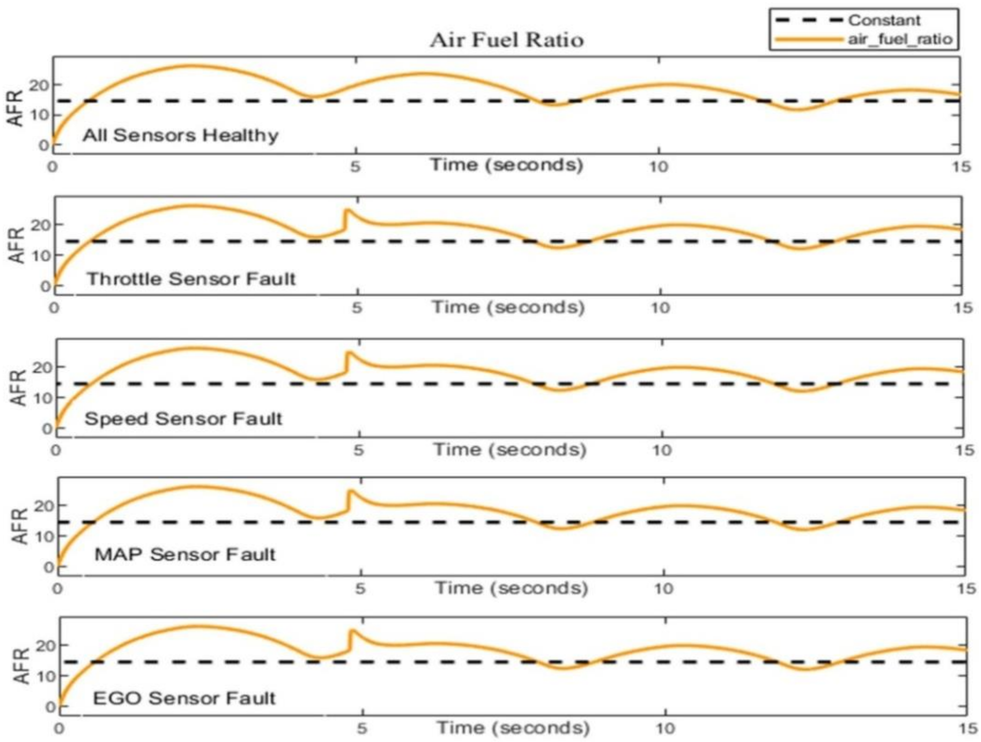

Figure 14. Performance of PFTCS.

The Matlab diagram of the proposed HFTCS is illustrated in Figure 15 by merging both controllers into the original model. The suggested HFTCS model includes both an FDI unit and an ST-SMC-based AFR robust controller. When faults were inserted one by one into each of the four sensors, the total performance of the HFTCS was as shown in Figure 16.

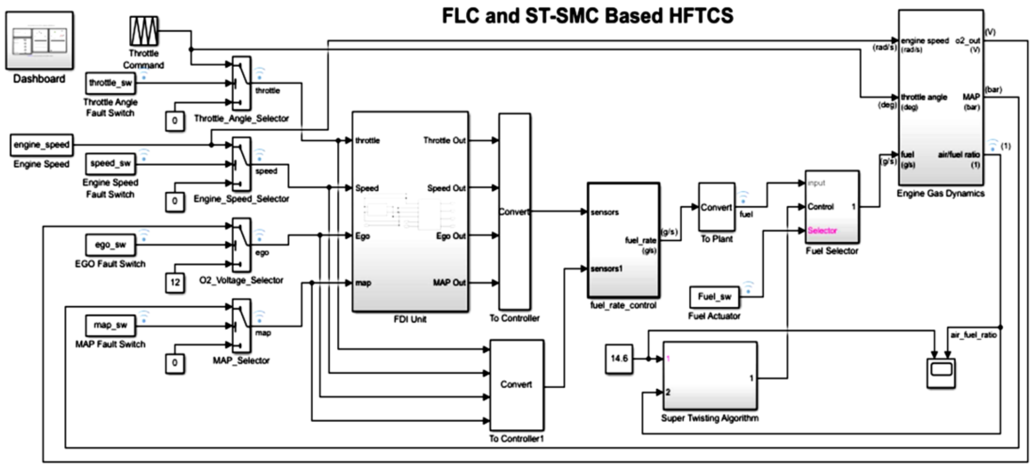

Figure 15. Matlab diagram of proposed HFTCS.

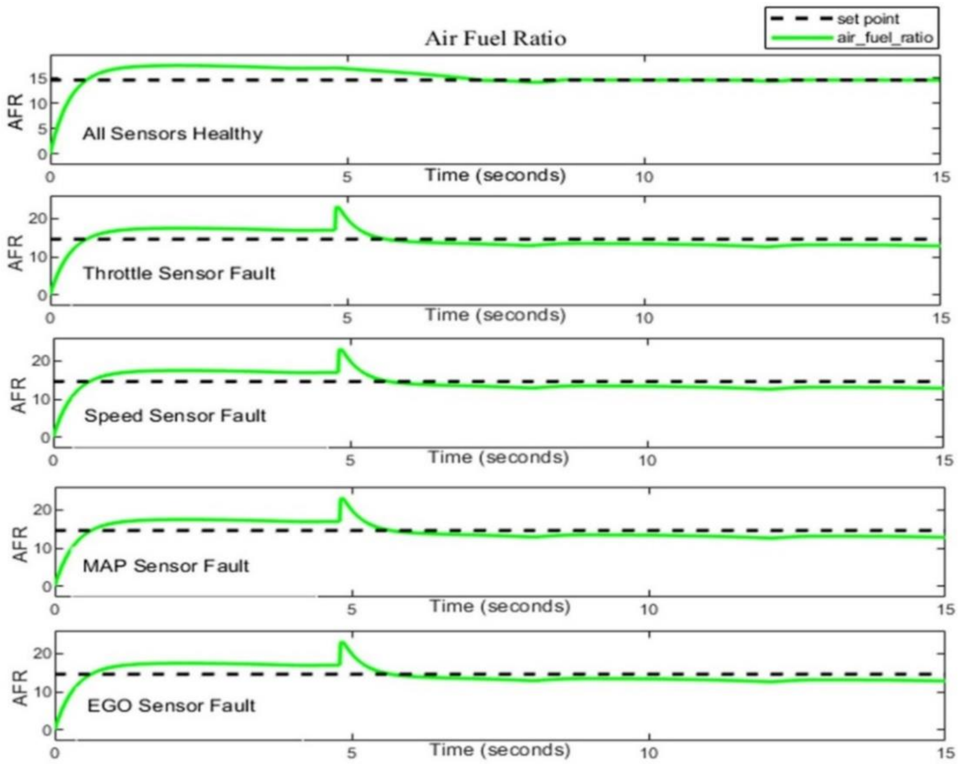

Figure 16. Overall performance of HFTCS.

The proposed HFTCS was fault-tolerant because the AFR value remained at 14.6. The suggested HFTCS provides several advantages over the existing models as explained in the next section.

4. Comparison with Previous Studies

In this section, the suggested design method is compared to other approaches that have been published. The original fault-tolerant MATLAB model [46] suffers from some important deficiencies. First, the existing MATLAB model lacks an appropriate FTC structure due to the absence of a distinct FDI unit. Our model has a suitable AFTCS architecture with a dedicated FDI unit. Second, the present methodology generates predicted sensor values from computationally inefficient lookup tables. Finally, the MATLAB model AFR degrades to 11.7 in faulty conditions, but the proposed model can maintain AFR in faulty conditions due to the addition of PFTCS using ST-SMC with reduced chattering effects.

Furthermore, AFTCS design has been studied using a variety of methods, including linear regression, LTs, the Kalman filter, artificial neural networks (ANNs), FL, and genetic algorithms (GA) [22–24,48–51]. The high computing costs of LTs, FL, and ANN are one of the methodologies' drawbacks with active compensation only. Due to the MAP sensor's narrow linear range, linear regression and KF were observed limited. To deal with highly nonlinear incorrect behavior, an enhanced robust control system was required. The HFTCS was analyzed using a PI controller in the passive part previously that caused excessive chattering with high misfires. The IC engine's AFR system's HFTCS system has never used this combination before. As a result, the proposed HFTCS provides a new FLC-based AFTCS for designing the FDI unit, as well as ST-SMC-based PFTCS architecture for masking faulty values. The performance of the FLC estimates for the AFTCS part is compared in Tables 2 and 3 [41]. These tables demonstrate that the MSE was minimized with the FLC technique for the throttle and MAP sensor estimations.

Table 2. MAP estimation using FLC-based observer [41].

Lookup Table Values	FLC Values	Error	MSE
0.091	0.10	−0.009	4.05×10^{-5}
0.113	0.11	0.003	4.5×10^{-6}
0.190	0.19	0	0
0.329	0.33	−0.001	5×10^{-7}
0.545	0.54	0.005	1.25×10^{-5}
0.745	0.74	0.005	1.25×10^{-5}
0.857	0.85	0.007	2.45×10^{-5}
0.915	0.91	0.005	1.25×10^{-5}
0.946	0.94	0.006	1.8×10^{-5}
0.964	0.96	0.004	8×10^{-6}
0.975	0.97	0.005	1.25×10^{-5}
0.985	0.99	−0.005	1.25×10^{-5}
0.994	0.99	0.004	8×10^{-6}
0.997	0.99	0.007	2.45×10^{-5}
0.998	0.99	0.008	3.2×10^{-5}
0.999	0.99	0.009	4.05×10^{-5}
0.999	0.99	0.009	4.05×10^{-5}

There are fewer advantages to single controllers than there are to hybrid controllers. Soft computing methods and fast processing speeds are further advantages that come with hybrid controllers. An FDI unit and a robust feedback controller were combined to produce a model for an ICE that is easier to utilize in both online and offline fault management. The model's implementation is quite easy compared to other techniques. The proposed HFTCS for ICEs was developed here due to all of these factors. A detailed comparison of the proposed approach with previously used approaches is provided in Table 4.

Table 3. Throttle estimation using FLC-based observer [41].

LT Values	FLC Values	Error	MSE
0	0.5	−0.5	1.25×10^{-1}
1.979	2.25	−0.271	3.6×10^{-2}
4.686	4.5	0.186	1.7×10^{-2}
6.258	6.25	0.008	3.2×10^{-5}
7.471	7.5	−0.029	4.2×10^{-4}
8.482	8.5	−0.018	1.6×10^{-4}
9.357	9.25	0.107	5.7×10^{-3}
10.163	10	0.163	1.3×10^{-2}
10.824	10.75	0.074	2.7×10^{-3}
11.452	11.5	−0.048	1.1×10^{-3}
12.061	12	0.061	1.8×10^{-3}
12.70	12.70	0	0
13.402	13.5	−0.098	4.8×10^{-3}
14.187	14.25	−0.063	1.9×10^{-3}
15.107	15.25	−0.143	1×10^{-2}
16.24	16.24	0	0
17.754	18	−0.246	3×10^{-2}

Table 4. Comparison of suggested approach with previous works [22–24,41,48–51].

Name of Controller	Major Drawback	Chattering Reduction	Degree of Robustness	Response Against Noise
Proposed HFTCS	-	Eliminates chattering effect	High and takes less time to respond	Best for noisy systems
HFTCS based on Kalman Filter	Linear range of sensors	Does not eliminate chattering	Moderate	High misfiring observed
HFTCS based on GA and HOSMC	Oscillations in AFR transient response	Better	High	High misfiring observed
AFTCS based on ANN and FLC	Comprises active part only	Does not eliminate chattering	Unknown duration for handling faults	High misfiring observed
AFTCS based on GA	Comprises active part only	Does not eliminate chattering	Unknown duration for handling faults	High misfiring observed
AFTCS based on Linear Regression	Linear range of sensors	Does not eliminate chattering	Not a robust technique	High misfiring observed

5. Conclusions

The HFTCS was proposed in this research for AFR control of IC engines using an FLC-based FDI unit in the active part to give approximated values to the controller during the sensor faults. An ST-SMC was developed as a passive part to adjust AFR in faulty scenarios by additionally adding the throttle actuator valve in the fuel supply line. The suggested HFTCS was designed in the available model of Matlab/Simulink to assure the reliability of an ICE. To examine the robustness of the novel HFTCS, faults were introduced into the sensors one by one. The results of the simulation indicate that the suggested system was stable and retained the desired AFR even when it was faulty. In faulty situations, it also maintained the AFR at 14.6 without any degradation, and a comparison with previous studies was also carried out to elaborate the benefits of the proposed HFTCS.

Future research might incorporate using a neuro-fuzzy system-based observer to cover the complete non-linear range of MAP while dealing with sensors' and actuators' partial faults with hardware-in-the-loop verifications. Integral sliding mode control (ISMC), a more advanced SMC method, can also be employed to improve robustness and performance.

Author Contributions: Conceptualization, A.A.A.; Formal analysis, U.R. and M.B.Q.; Funding acquisition, T.A.; Investigation, M.J.; Methodology, U.R. and A.A.A.; Project administration, A.A.A. and M.J.; Resources, M.B.Q.; Software, M.B.Q.; Supervision, T.A.; Validation, S.A.; Visualization, S.A.; Writing—original draft, U.R.; Writing—review & editing, A.A.A., S.A. and M.J. All authors have read and agreed to the published version of the manuscript.

Funding: This research was supported by the Deanship of Scientific Research at Najran University for funding this work under the Research Groups Funding program, grant code (NU/RG/SERC/11/5).

Data Availability Statement: This statement is not required in our paper as we do not report any data.

Acknowledgments: The authors are thankful to the Deanship of Scientific Research at Najran University for funding this work under the Research Groups Funding program, grant code (NU/RG/SERC/11/5).

Conflicts of Interest: The authors declare no conflict of interest in preparing this paper.

Abbreviations

Abbreviation	**Explanation**
FTC	Fault-Tolerant Control
ICE	Internal Combustion Engine
HFTCS	Hybrid Fault-Tolerant Control System
MAP	Manifold Absolute Pressure
MF	Membership Function
FDI	Fault Detection and Isolation
AFR	Air–fuel Ratio Control
FIU	Fault Injection Unit
MPC	Model Predictive Controller
LT	Lookup Table
ECU	Engine Control Unit
FIS	Fuzzy Inference System
PFTCS	Passive Fault-Tolerant Control System
EGO	Exhaust Gas Oxygen
AFTCS	Active Fault-Tolerant Control System
FLC	Fuzzy Logic Control
CI	Compression-Ignition
PID	Proportional Integral and Derivative
SI	Spark Ignition
CI	Compression-Ignition
FL	Fuzzy Logic
ISMC	Integral Sliding Mode Control
SMC	Sliding Mode Control
ST-SMC	Super Twisting Sliding Mode Control
Variable	Description of Variable
m_{air}	Mass of Air
$\overline{y}$	Estimated Output
T_{in}	Manifold Input Air Temperature
$\dot{m}_{fv}$	Vapor Fuel Flow
V_{in}	Manifold Input Air Volume
y_d	Desired Output
$\dot{m}_{Cyt}$	Mass Flow into Cylinders
α/β	Parameters of Engine
N_e	Engine Speed

E	Mean Square Error
ϕ_{th}	Throttle Opening Position
u	Actual Input
$S_{es}(\phi_{th})$	True Throttle Opening Position
$\dot{\lambda}(t)$	Lambda Sensor
τ_f	Fuel Vapor Process
γ	Heat Ratio of Air
$\dot{m}_f(t)$	Fuel Flow into Cylinders
C_d	Discharge Coefficient
$\ddot{m}_{ff}(t)$	Liquid Mass Fuel Flow
e_x	Residual
τ_λ	Time Delay
y	Actual Output
$\dot{m}_{th}$	Mass Flow Through Valve
x_1/x_2	State Variables
m_{fuel}	Mass of Fuel
$\overline{x}_1/\overline{x}_2$	Estimated Values of Observer Design
P_{in}	Manifold Input Air Pressure
η	Learning Rate
R	Gas Constant
sgn	Signum Function
r	Relative Degree Between u and y
$\mathrm{c_i}$	Arbitrary Positive Constant
tanh, sat	continuous functions
U	Control Boundary Value
σ_0	Boundary Layer
Φ, W, $\Gamma_{\mathrm{M}}, \mathrm{s_0}$	Positive Constants
$\mathrm{W}, \rho, \lambda$	Control Gains
$\dot{\mathrm{m}}_{\mathrm{ai}}$	Mass Flow Rate of Air Into Manifold
$\mathrm{P_m}$	Manifold Pressure
$\mathrm{P_{amb}}$	Ambient Pressure
θ	Throttle Angle
T	Temperature in Kelvin
$\mathrm{V_m}$	Volume of Manifold
$\dot{\mathrm{P}}_{\mathrm{m}}$	Rate of Change in Manifold Pressure
$\dot{\mathrm{m}}_{\mathrm{ao}}$	Mass Flow Rate of Air Out of Manifold
N	Sped of Engine
$\mathrm{V_{cd}}$	Cylinder Displacement Volume of Engine
ϑ	Volumetric Efficiency
$\mathrm{C_{pump}}$	Time-Varying Scale Factor
$\dot{\mathrm{m}}_{\mathrm{f}}$	Total Amount of Fuel
$\dot{\mathrm{m}}_{\mathrm{ff}}$	Feedforward Component of Fuel
$\dot{\mathrm{m}}_{\mathrm{fb}}$	Feedback Component of Fuel
$\mathrm{e_0, e_1, e_2}$	Intermediate Error Signals
β	Stoichiometric Ratio

References

1. Carbot-Rojas, D.A.; Escobar-Jiménez, R.F.; Gómez-Aguilar, J.F.; Téllez-Anguiano, A.C. A survey on modeling, biofuels, control and supervision systems applied in internal combustion engines. *Renew. Sustain. Energy Rev.* **2017**, *73*, 1070–1085. [CrossRef]
2. Lauber, J.; Khiar, D.; Guerra, T.M. Air-fuel ratio control for an IC engine. In Proceedings of the 2007 IEEE Vehicle Power and Propulsion Conference, Arlington, TX, USA, 9–12 September 2007; pp. 718–723.
3. Air Fuel Ratio–x-Engineer.org. Available online: https://x-engineer.org/air-fuel-ratio/ (accessed on 17 August 2022).
4. Hillier, V.A. *Fundamentals of Motor Vehicle Technology*. Stanley Thornes Ud P4-14. 1966, pp. 307–317. Available online: https://www.amazon.com/Fundamentals-Motor-Vehicle-Technology-Hillier/dp/0091431611 (accessed on 17 August 2022).
5. Muske, K.R. A model-based SI engine air fuel ratio controller. In Proceedings of the 2006 American Control Conference, Minneapolis, MN, USA, 14–16 June 2006; p. 6.
6. Amin, A.A.; Mahmood-ul-Hasan, K. Robust passive fault tolerant control for air fuel ratio control of internal combustion gasoline engine for sensor and actuator faults. *IETE J. Res.* **2021**, 1–16. [CrossRef]

7. Amin, A.A.; Mahmood-Ul-Hasan, K. Advanced fault tolerant air-fuel ratio control of internal combustion gas engine for sensor and actuator faults. *IEEE Access* **2019**, *7*, 17634–17643. [CrossRef]
8. Kim, J.; Chun, K.M.; Song, S.; Baek, H.-K.; Lee, S.W. Hydrogen effects on the combustion stability, performance and emissions of a turbo gasoline direct injection engine in various air/fuel ratios. *Appl. Energy* **2018**, *228*, 1353–1361. [CrossRef]
9. Chang, C.-F.; Fekete, N.P.; Amstutz, A.; Powell, J. Air-fuel ratio control in spark-ignition engines using estimation theory. *IEEE Trans. Control Syst. Technol.* **1995**, *3*, 22–31. [CrossRef]
10. Wang, S.; Yu, D.L. A new development of internal combustion engine air-fuel ratio control with second-order sliding mode. *J. Dyn. Syst. Meas. Control* **2007**, *129*, 757–766. [CrossRef]
11. Wu, H.-M.; Tafreshi, R. Fuzzy Sliding-mode Strategy for Air-fuel Ratio Control of Lean-burn Spark-Ignition Engines. *Asian J. Control* **2018**, *20*, 149–158. [CrossRef]
12. Li, Z.; Li, J.; Zhou, Q.; Zhang, Y.; Xu, H. Intelligent air/fuel ratio control strategy with a PI-like fuzzy knowledge-based controller for gasoline direct injection engines. *Proc. Inst. Mech. Eng. Part. J Automob. Eng.* **2018**, *233*, 2161–2173. [CrossRef]
13. Sui, W.; Hall, C.M. Combustion phasing modeling and control for compression ignition engines with high dilution and boost levels. *Proc. Inst. Mech. Eng. Part J. Automob. Eng.* **2019**, *233*, 1834–1850. [CrossRef]
14. Na, J.; Herrmann, G.; Rames, C.; Burke, R.; Brace, C. Air-fuel-ratio control of engine system with unknown input observer. In Proceedings of the 2016 UKACC 11th International Conference on Control (CONTROL), Belfast, UK, 31 August–2 September 2016; pp. 1–6.
15. Hendricks, E.; Sorenson, S.C. Mean value modelling of spark ignition engines. *SAE Trans.* **1990**, *99*, 1359–1373.
16. Meng, L.; Wang, X.; Zeng, C.; Luo, J. Adaptive air-fuel ratio regulation for port-injected spark-ignited engines based on a generalized predictive control method. *Energies* **2019**, *12*, 173. [CrossRef]
17. Li, L.; Luo, H.; Ding, S.X.; Yang, Y.; Peng, K. Performance-based fault detection and fault-tolerant control for automatic control systems. *Automatica* **2019**, *99*, 308–316. [CrossRef]
18. Amin, A.A.; Hasan, K.M. A review of fault tolerant control systems: Advancements and applications. *Measurement* **2019**, *143*, 58–68. [CrossRef]
19. Frank, P.M. Trends in fault-tolerant control of engineering systems. *IFAC Proc. Vol.* **2004**, *37*, 377–384. [CrossRef]
20. Butt, A.S.; Huda, N.U.; Amin, A.A. Design of fault-tolerant control system for distributed energy resources based power network using Phasor Measurement Units. *Meas. Control* **2022**. [CrossRef]
21. Wang, Y.; Zhou, D.; Qin, S.J.; Wang, H. Active fault-tolerant control for a class of nonlinear systems with sensor faults. *Int. J. Control Autom. Syst.* **2008**, *6*, 339–350.
22. Amin, A.A.; Mahmood-ul-Hasan, K. Unified Fault-Tolerant Control for Air-Fuel Ratio Control of Internal Combustion Engines with Advanced Analytical and Hardware Redundancies. *J. Electr. Eng. Technol.* **2022**, *17*, 1947–1959. [CrossRef]
23. Shahbaz, M.H.; Amin, A.A. Design of active fault tolerant control system for air fuel ratio control of internal combustion engines using artificial neural networks. *IEEE Access* **2021**, *9*, 46022–46032. [CrossRef]
24. Amin, A.A.; Mahmood-ul-Hasan, K. Robust active fault-tolerant control for internal combustion gas engine for air–fuel ratio control with statistical regression-based observer model. *Meas. Control* **2019**, *52*, 1179–1194. [CrossRef]
25. Chetouani, Y. Using the kalman filtering for the fault detection and isolation (FDI) in the nonlinear dynamic processes. *Int. J. Chem. React. Eng.* **2008**, *6*. [CrossRef]
26. Jiang, B.; Staroswiecki, M.; Cocquempot, V. Active fault tolerant control for a class of nonlinear systems. *IFAC Proc. Vol.* **2003**, *36*, 125–130. [CrossRef]
27. Kobayashi, T.; Simon, D.L. Application of a bank of Kalman filters for aircraft engine fault diagnostics. In Proceedings of the ASME Turbo Expo 2003, Collocated with the 2003 International Joint Power Generation Conference, Atlanta, GA, USA, 16–19 June 2003; Volume 36843, pp. 461–470.
28. Benosman, M. Passive fault tolerant control. In *Robust Control, Theory and Applications*; Bartoszewicz, A., Ed.; IntechOpen: London, UK, 2011. Available online: https://www.intechopen.com/chapters/15038 (accessed on 17 August 2022).
29. Murtaza, G.; Bhatti, A.I.; Butt, Y.A. Super twisting controller-based unified FDI and FTC scheme for air path of diesel engine using the certainty equivalence principle. *Proc. Inst. Mech. Eng. Part J. Automob. Eng.* **2018**, *232*, 1623–1633. [CrossRef]
30. Li, Y.; Tong, S. Fault diagnosis and fuzzy fault-tolerant control design of nonlinear systems with actuator faults. In Proceedings of the 2016 35th Chinese control conference (CCC), Chengdu, China, 27–29 July 2016; pp. 6512–6514.
31. Tang, L.; Ma, D.; Zhao, J. Neural networks-based active fault-tolerant control for a class of switched nonlinear systems with its application to RCL circuit. *IEEE Trans. Syst. Man Cybern. Syst.* **2018**, *50*, 4270–4282. [CrossRef]
32. Carbot-Rojas, D.A.; Escobar, R.F.; Gómez-Aguilar, J.F.; López-López, G.; Olivares-Peregrino, V.H. Experimental validation of an actuator fault tolerant control system using virtual sensor: Application in a double pipe heat exchanger. *Chem. Eng. Res. Des.* **2015**, *104*, 400–408. [CrossRef]
33. Alsuwian, T.; Amin, A.A.; Maqsood, M.T.; Qadir, M.B.; Almasabi, S.; Jalalah, M. Advanced Fault-Tolerant Anti-Surge Control System of Centrifugal Compressors for Sensor and Actuator Faults. *Sensors* **2022**, *22*, 3864. [CrossRef]
34. Su, S.W.; Bao, J.; Lee, P.L. A hybrid active–passive fault-tolerant control approach. *Asia-Pac. J. Chem. Eng.* **2006**, *1*, 54–62. [CrossRef]
35. Wang, J.; Yao, X.; Li, W. Hybrid active-passive robust fault-tolerant control of event-triggered nonlinear NCS. *Open Electr. Electron. Eng. J.* **2017**, *11*, 68–86. [CrossRef]

36. Mittal, K.; Jain, A.; Vaisla, K.S.; Castillo, O.; Kacprzyk, J. A comprehensive review on type 2 fuzzy logic applications: Past, present and future. *Eng. Appl. Artif. Intell.* **2020**, *95*, 103916. [CrossRef]
37. Ghassemi, A.; Scott, M.J. Investigating the role of renewable energies in integrated energy-water nexus planning under uncertainty using fuzzy logic. In *International Online Conference on Intelligent Decision Science*; Springer: Cham, Switzerland, 2020; pp. 696–702.
38. Feng, G. Controller synthesis of fuzzy dynamic systems based on piecewise Lyapunov functions. *IEEE Trans. Fuzzy Syst.* **2003**, *11*, 605–612. [CrossRef]
39. Khoei, A.; Hadidi, K.; Jamal, S.; Yuvarajan, S. Speed Control of a dc Motor using a New Fuzzy Controller. *IETE J. Res.* **2002**, *48*, 93–98. [CrossRef]
40. Li, Z.; Zhou, Q.; Zhang, Y.; Li, J.; Xu, H. Enhanced intelligent proportional-integral-like fuzzy knowledge-based controller using chaos-enhanced accelerated particle swarm optimization algorithm for transient calibration of air–fuel ratio control system. *Proc. Inst. Mech. Eng. Part D J. Automob. Eng.* **2020**, *234*, 39–55. [CrossRef]
41. Riaz, U.; Amin, A.A.; Tayyeb, M. Design of active fault-tolerant control system for Air-fuel ratio control of internal combustion engines using fuzzy logic controller. *Sci. Prog.* **2022**, *105*, 00368504221094723. [CrossRef] [PubMed]
42. Umar, R.; Muhammad, T.; Arslan, A.A. A Review of Sliding Mode Control with the Perspective of Utilization in Fault Tolerant Control. *Recent Adv. Electr. Electron. Eng.* **2021**, *14*, 312–324.
43. Seeber, R.; Horn, M.; Fridman, L. A novel method to estimate the reaching time of the super-twisting algorithm. *IEEE Trans. Autom. Control* **2018**, *63*, 4301–4308. [CrossRef]
44. Jamaludin, Z.; Puveneswaran, P.; Heng, C.T.; Maharof, M. Design and Application of ST-SMC Controller for Position Control of a Milling Table. In *Symposium on Intelligent Manufacturing and Mechatronics*; Springer: Singapore, 2021; pp. 236–246.
45. Levant, A. Sliding order and sliding accuracy in sliding mode control. *Int. J. Control* **1993**, *58*, 1247–1263. [CrossRef]
46. Modeling a Fault-Tolerant Fuel Control System-MATLAB & Simulink. Available online: https://www.mathworks.com/help/simulink/slref/modeling-a-fault-tolerant-fuel-control-system.html;jsessionid=15355714087914c0680043f8c298 (accessed on 22 April 2022).
47. Modeling Engine Timing Using Triggered Subsystems-MATLAB & Simulink. Available online: https://www.mathworks.com/help/simulink/slref/modeling-engine-timing-using-triggered-subsystems.html (accessed on 22 April 2022).
48. Amin, A.A.; Mahmood-ul-Hasan, K. Hybrid fault tolerant control for air–fuel ratio control of internal combustion gasoline engine using Kalman filters with advanced redundancy. *Meas. Control* **2019**, *52*, 473–492. [CrossRef]
49. Alsuwian, T.; Tayyeb, M.; Amin, A.A.; Qadir, M.B.; Almasabi, S.; Jalalah, M. Design of a Hybrid Fault-Tolerant Control System for Air–Fuel Ratio Control of Internal Combustion Engines Using Genetic Algorithm and Higher-Order Sliding Mode Control. *Energies* **2022**, *15*, 5666. [CrossRef]
50. Alsuwian, T.; Iqbal, M.S.; Amin, A.A.; Qadir, M.B.; Almasabi, S.; Jalalah, M. A Comparative Study of Design of Active Fault-Tolerant Control System for Air–Fuel Ratio Control of Internal Combustion Engine Using Particle Swarm Optimization, Genetic Algorithm, and Nonlinear Regression-Based Observer Model. *Appl. Sci.* **2022**, *12*, 7841. [CrossRef]
51. Iqbal, M.S.; Amin, A.A. Genetic algorithm based active fault-tolerant control system for air fuel ratio control of internal combustion engines. *Meas. Control* **2022**, 00202940221115233. [CrossRef]